RSC Advances

PAPER

View Article Online
View Journal | View Issue



Cite this: *RSC Adv.*, 2017, **7**, 44531

# Growth phase diagram and upconversion luminescence properties of $NaLuF_4$:$Yb^{3+}$/$Tm^{3+}$/$Gd^{3+}$ nanocrystals†

Yangyang Li,[a] Yanhui Dong,[a] Tuerxun·Aidilibike,[ab] Xiaohui Liu,[a] Junjie Guo[a] and Weiping Qin *[a]

Received 18th July 2017
Accepted 1st September 2017

DOI: 10.1039/c7ra07902h

rsc.li/rsc-advances

Sub-25 nm β-$NaLuF_4$ nanocrystals (NCs) with high homogeneity, monodispersity, and good crystallinity were synthesized through thermal decomposition at different temperatures (285, 295, 305, and 315 °C), using an automatic nanomaterial synthesizer. The phase transition of $NaLuF_4$ NCs from α-phase to β-phase suggests that the entire growth process consists of four stages: a cubic phase, the coexistence of cubic and hexagonal phases, a homogeneous hexagonal phase, and an inhomogeneous hexagonal phase, caused by Ostwald ripening. Based on this observation, we obtained the growth phase diagram of $NaLuF_4$:$Yb^{3+}$/$Tm^{3+}$/$Gd^{3+}$ NCs, relating to the reaction time, temperature, crystal size, and crystal phase. From spectral analysis, the products prepared in the third stage were shown to exhibit the characteristics of having small size (sub-25 nm), uniformity, and high upconversion luminescence (UCL) intensity. On the other hand, the luminescence properties of $NaLuF_4$:$Yb^{3+}$,$Tm^{3+}$ were studied *via* incorporating different concentrations of $Gd^{3+}$ ions. These results indicated that 10% $Gd^{3+}$ was the best doping concentration for obtaining $NaLuF_4$ NCs with relatively small size and high brightness. Further increasing the $Gd^{3+}$ concentration induced a drastic decrease in UCL intensity.



## Introduction

Rare earth (RE) doped nanomaterials have received considerable interest due to their potential applications in optics, microelectronics, optoelectronics, and biomedical sciences, because of their unique optical properties.[1–3] In recent years, scientists have paid much attention to typical RE doped $NaREF_4$ materials due to their potential applications in solid-state lasers, bioimaging, photodynamic therapy, *etc.*[4–11] As a commonly studied object, β-$NaYF_4$ was acknowledged as the most efficient UC host material before 2011.[12–14] However, Qin and co-workers reported that β-$NaLuF_4$:18% $Yb^{3+}$,0.5% $Tm^{3+}$ exhibited more intense ultraviolet and blue UC luminescence than β-$NaYF_4$:18% $Yb^{3+}$,0.5% $Tm^{3+}$ of the same size.[15] As a typical RE doped $NaREF_4$ material, β-$NaLuF_4$ may be a more promising host for UC behavior than β-$NaYF_4$, especially for high-order multi-photon UCL. Furthermore, it is generally accepted that β-phase $NaLuF_4$ provides much stronger UCL compared with its α-phase counterpart.[12,16] Meanwhile, the hexagonal form of $NaLuF_4$ usually appears with larger nanoparticles than the cubic form.[7,17,18] Appropriate size and good luminescence properties are the fundamental requirements for the application of UC nanomaterials to bioimaging, biotherapy, bioassaying, *etc.* Hence it is of great significance to prepare small size and high brightness β-$NaLuF_4$ for biological applications. However, as we know, there is still no established approach for discussing the growth process of $NaLuF_4$ NCs. Therefore, a clear growth phase diagram of $NaLuF_4$ NCs will be helpful for obtaining the desired $NaLuF_4$ nanomaterials.

In general, nanocrystal size can be controlled by adjusting the raw material ratio, reaction time, and reaction temperature. During the past decade, impurity doping technologies have become a research hotspot because of their significant role in modifying morphology and decreasing size in many nanomaterials, which has been demonstrated by some groups.[17,19–25] For instance, Li *et al.* reported that the doping of 24 mol% $Gd^{3+}$ ions could control the size of lanthanide-doped $NaLuF_4$ nanocrystals to sub-10 nm.[20] Doping $Gd^{3+}$ ions in an $NaLuF_4$ host lattice can reduce the size of the nanocrystals, but meanwhile it will also reduce their luminescence performance. However, this weakness has been rarely mentioned in relevant reports. Therefore, research consideration must be given to the balance between crystal size and luminescence performance in order to obtain high-quality $NaLuF_4$ nanomaterials. At present, the thermal decomposition method has been widely used in the preparation of $NaREF_4$ nanomaterials.[26–30] The advantages of

[a]*State Key Laboratory on Integrated Optoelectronics, College of Electronic Science and Engineering, Jilin University, Changchun, Jilin 130012, China. E-mail: wpqin@jlu.edu.cn*

[b]*Yili Normal University, Electronic and Information Engineering, Yining, Xinjiang 835000, China*

† Electronic supplementary information (ESI) available: Additional results of TEM, SEM, XRD and UC spectra. See DOI: 10.1039/c7ra07902h

this method are the shorter experimental time and that it is easier to get small size products compared with the traditional hydrothermal method. Thermolysis usually requires a higher temperature, resulting in crystal growth rate that is faster and more sensitive to external factors than when using hydrothermal methods. For this reason, it is hard to ensure the uniqueness of experimental variables and the repeatability of products during parallel synthesis. However, these problems can be easily resolved for us through the use of an independently-developed automatic nanomaterial synthesizer (ANS02, Changchun Micro Era Technology Co. LTD.). With the help of this instrument, all experimental parameters, such as the heating rate, stirring speed, air flow rate, and dropping rate of the sodium source and fluoride source, can be exactly set in a computer program. Therefore, it provides technical support for precise research into the growth and phase transition processes for nanocrystals.

Herein, we studied the nucleation, phase transition, Ostwald ripening, and luminescence properties of $NaLuF_4$ nanocrystals through precisely changing experimental parameters. According to the effects of different reaction times and temperatures on the growth processes of $NaLuF_4$ crystals, we obtained a time–temperature–phase–size (T–T–P–S) phase diagram. Combined with spectral analysis, these results indicate that material with small size, uniform shape, monodispersity, and high UCL intensity can be obtained in a specific region of the diagram at any temperature from 285 to 315 °C. In addition, we investigated the influence of $Gd^{3+}$ ions on the sizes of the crystals and the luminescence properties of $NaLuF_4$:$Yb^{3+}$,$Tm^{3+}$,$Gd^{3+}$ nanomaterials. It was found that a high concentration of $Gd^{3+}$ could drastically reduce the luminescence performance of $NaLuF_4$, and the doping of 10 mol% $Gd^{3+}$ is suitable for the preparation of this nanomaterial with relatively small size and strong upconversion emission.

## Results and discussion

Using the automatic nanomaterial synthesizer mentioned above, $NaLuF_4$:20% $Yb^{3+}$,0.5% $Tm^{3+}$,*x*% $Gd^{3+}$ ($x = 0$, 3, 5, 10, 20, or 30) NCs were obtained at 305 °C *via* a thermal decomposition method. The morphologies and sizes of the nanocrystals were characterized *via* TEM, as shown in Fig. 1. In Fig. 1a–c, the nanocrystals with lower doped amounts of $Gd^{3+}$ ions are relatively large and irregular, while the sample with a $Gd^{3+}$ doping concentration of 10% shows a uniform and regular shape with an average diameter of around 23 nm and a narrow size distribution (Fig. 1d and g). Increasing the amount of $Gd^{3+}$ ions to 30%, the crystal size becomes non-uniform again, with a larger distribution varying from 7–12 nm (Fig. 1f and g). Here, we found that an increase in the doping amount of $Gd^{3+}$ ions has obvious modifying effects on the growth of the nanocrystals. Combined with the results from XRD studies (Fig. S1†), these effects mainly show in two aspects: the decrease in crystal size; and the crystal shape changing, following the order irregularity–regularity–irregularity.

In order to study the influence of $Gd^{3+}$ concentration on the crystal size and UCL properties of $NaLuF_4$, relevant data are plotted in Fig. 2. The UCL intensity decreased obviously with an increase in $Gd^{3+}$ concentration. This decrease can attributed to two factors: a decrease in crystal size and the reduced luminescence performance of the material from introducing $Gd^{3+}$ into the $NaLuF_4$ host lattice. Compared with the UCL intensity

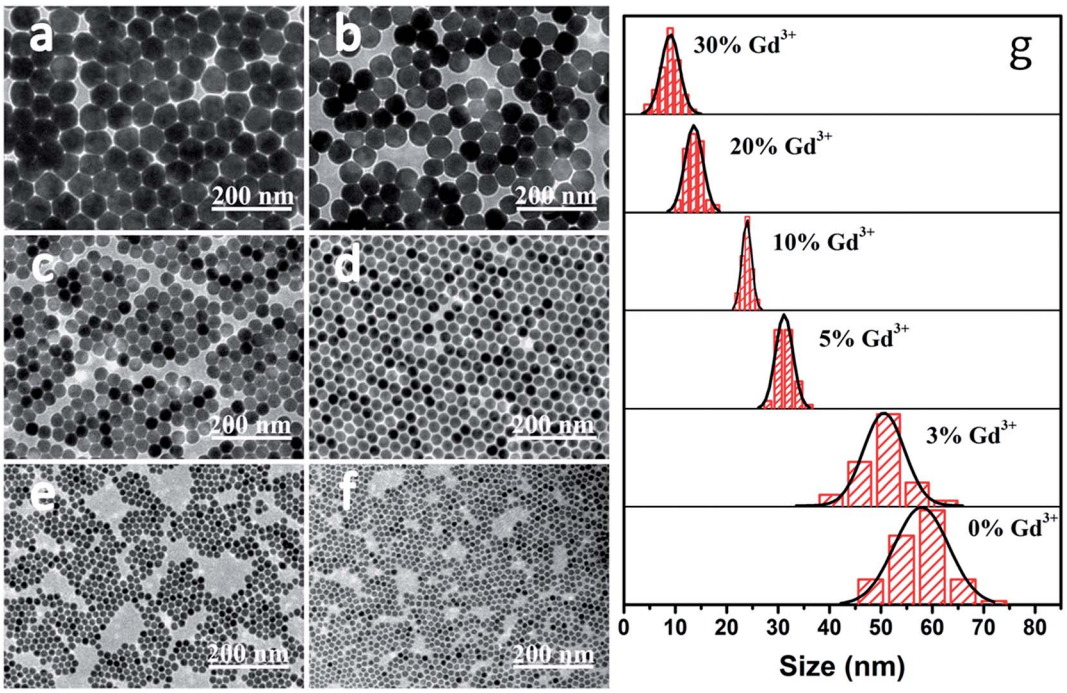


Fig. 1 TEM images of $NaLuF_4$:20% $Yb^{3+}$,0.5% $Tm^{3+}$,*x*% $Gd^{3+}$ with (a) $x = 0$, (b) $x = 3$, (c) $x = 5$, (d) $x = 10$, (e) $x = 20$, and (f) $x = 30$. (g) Size distributions of the aforementioned NCs.

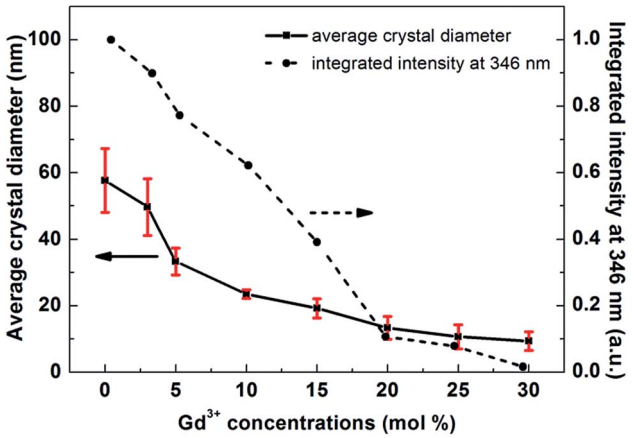


Fig. 2 Average crystal diameters and relative UCL integrated intensities at 346 nm for $NaLuF_4$:20% $Yb^{3+}$,0.5% $Tm^{3+}$,*x*% $Gd^{3+}$ NCs, both with respect to $Gd^{3+}$ doping concentration. The error bars represent the difference in size between the largest crystal and the smallest one in our statistical results.

at 346 nm for a sample with no $Gd^{3+}$, the luminescence intensities of samples with larger amounts of $Gd^{3+}$ (3%, 5%, and 10%) decreased by 10.1%, 22.7% and 37.8%, respectively. Meanwhile, the average crystal size decreased by 61%, from 59 nm to 23 nm. There is a similar dependence of crystal size, as well as UCL, on $Gd^{3+}$ concentration, indicating the dominant role of size on the UCL decrease. Upon increasing the $Gd^{3+}$ concentration to 15, 20, 25 and 30%, the average crystal sizes are 19, 13, 10, and 9 nm, respectively. The corresponding UCL intensities of samples were calculated to be 39.2, 10.7, 7.9, and 1.6% of the value for $NaLuF_4$:20% $Yb^{3+}$,0.5% $Tm^{3+}$ NCs. It can be seen that these UCL intensities decrease significantly upon a relatively small change in size and a large change in $Gd^{3+}$ concentration. Contrary to the decrease in UCL intensity for samples with smaller amounts of $Gd^{3+}$ ions, a degradation in material performance due to a relatively large amount of $Gd^{3+}$ ions may be the main factor for this drastic decrease. To further verify that $Gd^{3+}$ can reduce the luminescence performance of $NaLuF_4$, we annealed the $Gd^{3+}$ variable samples to eliminate the effects of size variation on luminescence performance. SEM images and UCL spectra from these annealed samples are shown in Fig. S2 and S3.† These samples exhibit similar irregular morphologies and sizes, but show obvious differences in spectral properties. The UCL intensities of the samples have a downward trend as the amount of $Gd^{3+}$ increases, especially in the UV region, but this trend is not obvious for samples with low $Gd^{3+}$ doping (≤10 mol%). In general, high-order multi-photon emission should be an important feature of a good upconversion material. Thus, too many $Gd^{3+}$ ions entering $Lu^{3+}$ sites will reduce the optical performance of $NaLuF_4$ nanomaterials. To summarize, it is remarkable that 10 mol% $Gd^{3+}$ is highly favorable for the preparation of high-quality hexagonal-phase $NaLuF_4$ nanocrystals with relatively small size, uniform shape, and high UCL intensity. Therefore, we maintain this doping ion concentration for the following discussion.

Fig. 3 demonstrates the effects of reaction time on the crystal growth and nucleation processes, while other parameters were kept unchanged. Here, the reaction time was regarded as the only variable factor, because all the experimental steps can be precisely controlled by setting them into computer programs, including the stirring speed, air flow rate, and dropping rate of the sodium source and fluoride source. A typical TEM image (Fig. 3a) demonstrates that the $NaLuF_4$ nanocrystals obtained at high temperature for 10 minutes have a pure cubic phase, which can also be seen from Fig. S2a.† The images in Fig. 3b–f and the XRD patterns in Fig. S2b–f† show the gradual phase transition of $NaLuF_4$ from a cubic phase to a hexagonal phase. In these, α-phase and β-phase NCs are coexistent and the proportion of the latter increases gradually over the first four

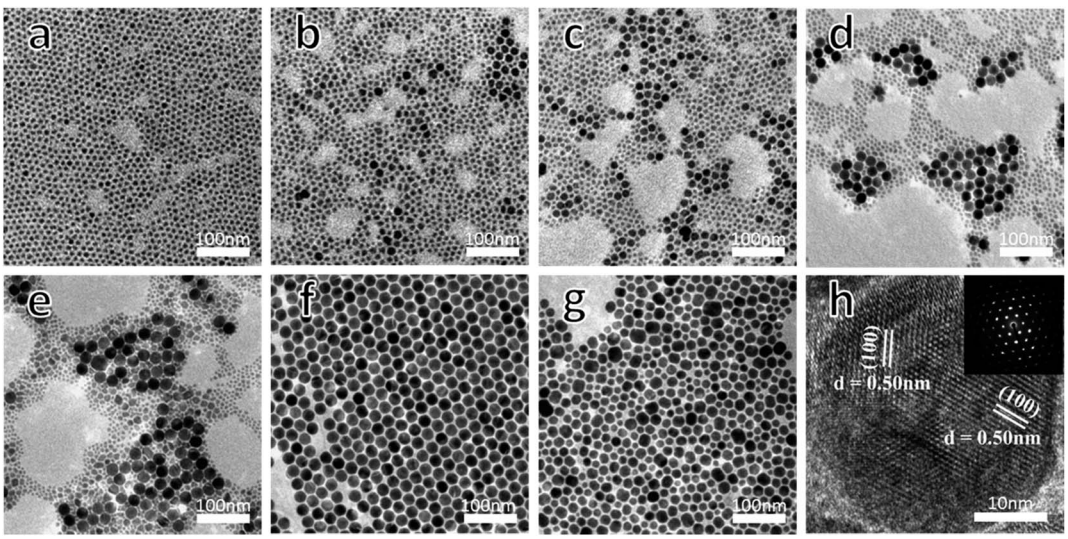


Fig. 3 TEM images of $NaLuF_4$:20% $Yb^{3+}$,0.5% $Tm^{3+}$,10% $Gd^{3+}$ synthesized at 305 °C for different reaction times of (a) 10 min, (b) 15 min, (c) 17 min, (d) 19 min, (e) 21 min, (f) 23 min, and (g) 65 min; and (h) a HRTEM image and selected area electron diffraction (SAED) pattern from the hexagonal NCs shown in (f).

pictures (Fig. 3b–e), which is consistent as well with the XRD results. It is worth noting that the $NaLuF_4$ NCs in Fig. 3f (23 min) show monodispersity and high uniformity. All these NCs display uniform hexagonal shape, with an average diameter of 23 nm, and a rather narrow size distribution, which indicates that a heat reaction time of about 23 minutes can result in the complete formation of pure β-phase $NaLuF_4$ using the current technology. HRTEM (Fig. 3h) characterization also provides further evidence that interplanar spacing of 0.50 nm can be indexed as being from (100) lattice fringes of β-phase $NaLuF_4$. TEM images of all samples prepared between 23 and 60 minutes (Fig. S5†) show samples similar in size and shape to that shown in Fig. 3f. This may be due to an ionic equilibrium state of free ions in the solvent, which leads to crystal growth at a relatively stable stage. Therefore, this time period is ideal for synthesizing β-$NaLuF_4$ with small size and high uniformity. Upon further prolonging the reaction time to 65 minutes, some of the crystals grow larger at the expense of smaller ones, which is known as Ostwald ripening (Fig. 3g). Ripening typically leads to a broadening of the size distribution, however, nanocrystals with a large size distribution are not as we expected. Therefore, the reaction time should not exceed 65 minutes under the current experimental conditions. The effects of reaction time on the phase and size of $NaLuF_4$ NCs are listed in Table 1.

To reveal the phase change and growth processes of $NaLuF_4$ NCs in detail, the same time-varying experiments were done at different temperatures of 285, 295 and 315 °C, and the relevant TEM images are shown in Fig. S6–S8,† respectively. The nucleation processes of $NaLuF_4$ NCs at different reaction temperatures can be seen in these TEM images. In order to facilitate comparison and analysis, we plotted a T–T–P–S phase diagram (Fig. 4) that could indicate the relationship between size, phase, temperature and reaction time. The phase transition process for $NaLuF_4$ NCs can be divided into four parts: a cubic phase, the coexistence of cubic and hexagonal phases, a homogeneous hexagonal phase, and an inhomogeneous hexagonal phase caused by Ostwald ripening. This phase diagram, on the whole, demonstrates that the higher the temperature, the faster the growth rate of the nanocrystals. In the first two stages, the crystal size increases monotonically, because of the phase transition from α-phase to β-phase. Notably, small and homogeneous β-$NaLuF_4$ NCs (sub-25 nm) can be obtained after different time periods, corresponding to different temperatures from 285 to 315 °C. Upon increasing the reaction temperature, the length of the third stage gradually becomes shorter: from 110 min to 280 min at 285 °C, from 60 min to 160 min at 295 °C, from 23 min to 65 min at 305 °C, and from 12 min to 30 min at 315 °C. It is generally accepted that hexagonal-phase

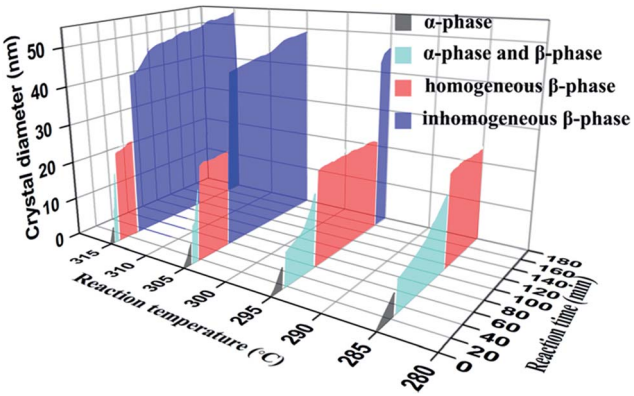


Fig. 4 Growth phase diagram of $NaLuF_4$:20% $Yb^{3+}$,0.5% $Tm^{3+}$,10% $Gd^{3+}$. Relationships between size, phase, temperature, and reaction time for the growth process of $NaLuF_4$ nanocrystals are shown.

nanocrystals show more efficient UCL than their cubic-phase counterparts, thus, this result is meaningful for preparing high-quality β-$NaLuF_4$ nanomaterials. Moreover, it is interesting to find that β-phase NCs prepared at different temperatures have similar dimensions of about 23 nm (Fig. S6e, S7e, 3f, and S8c†), which indicates that temperature mainly affects the growth rate, while the raw material ratio mainly affects the shape and size of $NaLuF_4$ nanocrystals. Further increasing the reaction time would lead to the ripening of the nanocrystals, resulting in inhomogeneous nanocrystals with a rather large size distribution. Ripened nanoparticles are not suitable for biological applications. In contrast, for materials prepared in the third stage, nanocrystals with small and uniform size have been found to show greater potential for applications.[31] Therefore, we have obtained synthetic details for small and homogeneous β-$NaLuF_4$ NCs, which may be further generalized to synthesize other ideal RE fluoride nanomaterials.

In order to characterize the luminescence properties of samples at various stages, we collected upconversion emission spectra from the as-obtained $NaLuF_4$:20% $Yb^{3+}$,0.5% $Tm^{3+}$,10% $Gd^{3+}$ NCs at 305 °C after different reaction times, as shown in Fig. 5. It can be seen that the overall luminescence intensities of the samples increase monotonically upon increasing the reaction time, under near infrared irradiation at 980 nm. A comparison of the intensities of emission at 346 nm shows that the UCL intensity of β-$NaLuF_4$ (23 min) is increased about 17-fold when compared to that of pure α-$NaLuF_4$ (10 min). This significant UCL enhancement in the β-$NaLuF_4$ NCs comes from their more ordered hexagonal structure and larger crystal size. As can be seen in the spectra, there are six main emission peaks

Table 1 Effects of reaction time on $NaLuF_4$ synthesis when other reaction conditions remain unchanged

| Reaction time/minutes | Phase | Size |
|---|---|---|
| 10 | Cubic | Very tiny |
| 15–21 | Cubic/hexagonal | Very tiny cubic phase and hexagonal phase, with diameters between 12 and 24 nm |
| 23–60 | Homogeneous hexagonal | ~23 nm |
| 65 | Inhomogeneous hexagonal | 7–53 nm |

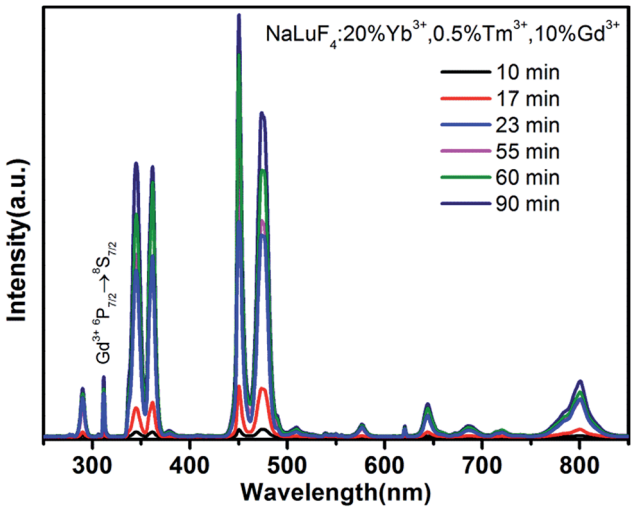


Fig. 5 Upconversion emission spectra of $NaLuF_4$:20% $Yb^{3+}$,0.5% $Tm^{3+}$,10% $Gd^{3+}$ synthesized at 305 °C after different reaction times under 980 nm near-infrared excitation.

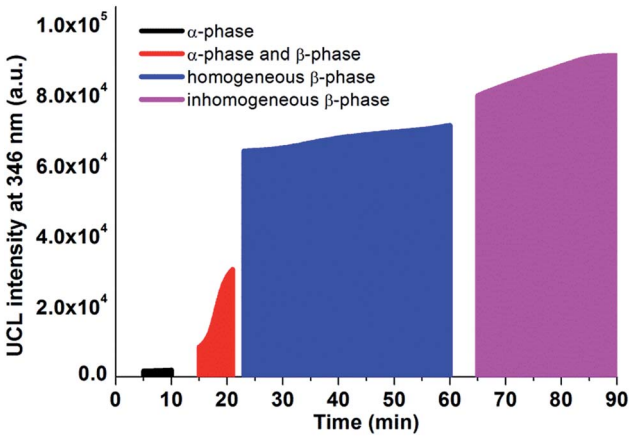


Fig. 6 The UCL integrated intensity at 346 nm and the crystal phase distribution of $NaLuF_4$:20% $Yb^{3+}$,0.5% $Tm^{3+}$,10% $Gd^{3+}$ synthesized at 305 °C, both with respect to reaction time.

at 290, 346, 361, 451, 474, and 801 nm, which are assigned to the $^1I_6 \rightarrow {}^3H_6$, $^1I_6 \rightarrow {}^3F_4$, $^1D_2 \rightarrow {}^3H_6$, $^1D_2 \rightarrow {}^3F_4$, $^1G_4 \rightarrow {}^3H_6$, and $^3H_4 \rightarrow {}^3H_6$ transitions of $Tm^{3+}$, respectively. In addition, the peak at 311 nm corresponds to the $^6P_{7/2} \rightarrow {}^8S_{7/2}$ transition of $Gd^{3+}$, which is a five-photon UCL process sensitized by $Tm^{3+}$.[32] Under 980 nm laser excitation, the emission spectra of all the as-synthesized samples were measured and all showed intensive high-order multi-photon UCL in the ultraviolet and near ultraviolet regions. Taking $NaLuF_4$ synthesized at 60 min as an example, the ratios of $I_{290}/I_{801}$, $I_{311}/I_{801}$, $I_{346}/I_{801}$, and $I_{361}/I_{801}$ ($I$ represents the intensity of the emission peak) are 1, 1.2, 4.3, and 4.7, respectively. Apart from the traditional application to *in vivo* imaging, using the intense emission of $Tm^{3+}$ at 801 nm,[33,34] our nanomaterials exhibit other excellent characteristics and may have a wider range of applications. Among the upconverted UV luminescence signals, the intense emissions at 346 and 361 nm are useful for activating UV-sensitive materials. Therefore, our investigations focus on the relationship between the UCL intensity at 346 nm and crystal phase of $NaLuF_4$:20% $Yb^{3+}$,0.5% $Tm^{3+}$,10% $Gd^{3+}$, as shown in Fig. 6.

Hexagonal-phase nanocrystals usually exhibit higher luminescence efficiency than their cubic-phase counterparts. The samples prepared in the α-phase stage show poor luminescence properties. If we define the UCL intensity (346 nm) of a sample prepared after 90 min as 100%, the intensity of the α-$NaLuF_4$ NCs is only about 2%. In the second stage, the UCL intensities of the samples increase rapidly due to the phase transition from the α-phase to β-phase. This phase transition leads to an increase in the UCL intensities of the time-varying samples from 9% to 33%. There is obvious spectral enhancement when the α-phase disappears completely and a pure and homogeneous β-phase is formed. The materials prepared in the period between 23 and 60 minutes have similar crystal sizes, and show a moderate increase in their luminescence intensity (from 70% to 78%) with an increase in reaction time. This is probably because the crystals obtained after a longer reaction time have higher crystallinity and a slightly larger size. Prolonging the reaction time over 65 minutes would lead to Ostwald ripening and cause a larger average size and broader size distribution. As indicated in Fig. 6, there is no significant enhancement in emission intensity after 65 minutes compared with the homogeneous β-$NaLuF_4$ material. Consequently, high-quality $NaLuF_4$ can be obtained in the third stage of the graph, and samples with a longer crystallization time have better luminescence properties.

## Conclusions

In this work, a series of $NaLuF_4$ nanomaterials were prepared using an automatic nanomaterial synthesizer to precisely control the experimental parameters. First we discussed the influence of varying the $Gd^{3+}$ doping amount on the size and UCL properties of $NaLuF_4$:$Yb^{3+}$,$Tm^{3+}$,$Gd^{3+}$. It has been shown that 10 mol% doping of $Gd^{3+}$ can be used to prepare $NaLuF_4$ NCs with relatively small size (sub-25 nm) and strong UCL intensity. Although higher $Gd^{3+}$ concentrations can produce smaller sized $NaLuF_4$ NCs, their UCL intensities are greatly decreased. Based on this observation, and combined with a large number of experimental results, we obtained the T–T–P–S phase diagram for $NaLuF_4$:20% $Yb^{3+}$,0.5% $Tm^{3+}$,10% $Gd^{3+}$ over the range from 285 to 315 °C. This phase diagram can guide us in the synthesis of samples with definite properties, in order to obtain the desired $NaLuF_4$ nanomaterials. For example, sub-25 nm β-$NaLuF_4$ NCs with uniform shape, monodispersity, and high UCL intensity can be obtained in the homogeneous β-phase regions of the diagram. More importantly, the phase diagram may be further generalized to study the growth progress of other $NaREF_4$ NCs.

## Experimental section

β-$NaLuF_4$:20% $Yb^{3+}$,0.5% $Tm^{3+}$,$x$% $Gd^{3+}$ nanocrystals were synthesized *via* a thermal decomposition method. The combined amount of $RECl_3 \cdot 6H_2O$ (RE = Lu, Yb, Tm, Gd) was

set to 2 mmol in total, and the next step was to mix $RECl_3 \cdot 6H_2O$ with 12 ml of oleic acid and 30 ml of 1-octadecene and add this into a three-neck flask. The mixture was heated to 160 °C and kept at this temperature for 30 min under dry argon; it was then cooled down to room temperature. After that, 10 ml of methanol solution containing NaOH (5 mmol) and 20 ml of methanol solution containing $NH_4F$ (8 mmol) were slowly dropped into the flask with constant stirring for 30 min. Then the reaction temperature was raised to 108 °C and maintained at this temperature for 20 min under a vacuum environment to remove the methanol. Finally, the solution was heated rapidly to the heating temperature (285 °C, 295 °C, 305 °C, or 315 °C) and kept at this temperature for a different number of minutes for each kind of product. It is worth noting that all of the above steps were automatically completed using the automatic nanomaterial synthesizer.

The samples were characterized *via* transmission electron microscopy (TEM), using an H-600 microscope at an acceleration voltage of 100 kV. High-resolution TEM (HRTEM) characterization was performed with a JEM-2200FS operated at 200 kV. The powder X-ray diffraction (XRD) patterns were recorded using a Model Rigaku Ru-200b diffractometer, using Cu K$\alpha$ radiation ($\lambda = 0.15406$ nm) in the 2-theta range from 10° to 70°. Power adjustable and continuous wave (CW) laser diodes (980 nm, 3 W) and a Hitachi F-4500 fluorescence spectrophotometer (PMT voltage is 400 V) were employed for upconversion spectral analysis. The spectral scan range was from 250 to 850 nm, with a resolution of 1 nm.

## Conflicts of interest

There are no conflicts to declare.

## Acknowledgements

This work was supported by the National Natural Science Foundation of China (11274139).

## References

1 J. Zhou, Z. Wu, Z. Zhang, W. Liu and H. Dang, *Wear*, 2001, **249**, 333–337.
2 X. Wang and Y. Li, *Angew. Chem., Int. Ed.*, 2003, **42**, 3497–3500.
3 S. Sivakumar, F. C. M. van Veggel and M. Raudsepp, *J. Am. Chem. Soc.*, 2005, **127**, 12464–12465.
4 A. Cooke, D. Jones, J. Silva and M. Wells, *J. Phys. C: Solid State Phys.*, 1975, **8**, 4083.
5 B. Choi, B. Moon, H. Seo, J. Jeong, H. Lee and W. Seo, *Mater. Des.*, 2000, **21**, 567–570.
6 S. Ghosh, T. Rosenbaum, G. Aeppli and S. Coppersmith, *Nature*, 2003, **425**, 48–51.
7 S. Heer, K. Kömpe, H. U. Güdel and M. Haase, *Adv. Mater.*, 2004, **16**, 2102–2105.
8 L. Liang, H. Xu, Q. Su, H. Konishi, Y. Jiang, M. Wu, Y. Wang and D. Xia, *Inorg. Chem.*, 2004, **43**, 1594–1596.
9 G. Yi, H. Lu, S. Zhao, Y. Ge, W. Yang, D. Chen and L.-H. Guo, *Nano lett.*, 2004, **4**, 2191–2196.
10 M. Karbowiak, A. Mech, A. Bednarkiewicz, W. Stręk and L. Kępiński, *J. Phys. Chem. Solids*, 2005, **66**, 1008–1019.
11 J. H. Zeng, J. Su, Z. H. Li, R. X. Yan and Y. D. Li, *Adv. Mater.*, 2005, **17**, 2119–2123.
12 K. W. Kramer, D. Biner, G. Frei, H. U. Gudel, M. P. Hehlen and S. R. Luthi, *Chem. Mater.*, 2004, **16**, 1244–1251.
13 Y. Wei, F. Lu, X. Zhang and D. Chen, *Chem. Mater.*, 2006, **18**, 5733–5737.
14 Z. Li and Y. Zhang, *Nanotechnology*, 2008, **19**, 345606.
15 F. Shi, J. Wang, X. Zhai, D. Zhao and W. Qin, *CrystEngComm*, 2011, **13**, 3782–3787.
16 G. Wang, Q. Peng and Y. Li, *J. Am. Chem. Soc.*, 2009, **131**, 14200–14201.
17 F. Wang, Y. Han, C. S. Lim, Y. Lu, J. Wang, J. Xu, H. Chen, C. Zhang, M. Hong and X. Liu, *Nature*, 2010, **463**, 1061–1065.
18 C. Li, J. Yang, P. Yang, X. Zhang, H. Lian and J. Lin, *Cryst. Growth Des.*, 2008, **8**, 923–929.
19 G. Xiang, J. Zhang, Z. Hao, X. Zhang, Y. Luo, S. Lü and H. Zhao, *CrystEngComm*, 2014, **16**, 2499–2507.
20 Q. Liu, Y. Sun, T. Yang, W. Feng, C. Li and F. Li, *J. Am. Chem. Soc.*, 2011, **133**, 17122–17125.
21 A. Xia, M. Chen, Y. Gao, D. Wu, W. Feng and F. Li, *Biomaterials*, 2012, **33**, 5394–5405.
22 S. Zeng, J. Xiao, Q. Yang and J. Hao, *J. Mater. Chem.*, 2012, **22**, 9870–9874.
23 D. Chen and Y. Wang, *Nanoscale*, 2013, **5**, 4621–4637.
24 Y. Chen, X. Yan, Q. Liu and X. Wang, *J. Alloys Compd.*, 2013, **562**, 99–105.
25 J. A. Damasco, G. Chen, W. Shao, H. Ågren, H. Huang, W. Song, J. F. Lovell and P. N. Prasad, *ACS Appl. Mater. Interfaces*, 2014, **6**, 13884–13893.
26 H.-X. Mai, Y.-W. Zhang, R. Si, Z.-G. Yan, L.-d. Sun, L.-P. You and C.-H. Yan, *J. Am. Chem. Soc.*, 2006, **128**, 6426–6436.
27 G. S. Yi and G. M. Chow, *Adv. Funct. Mater.*, 2006, **16**, 2324–2329.
28 C. Liu, H. Wang, X. Zhang and D. Chen, *J. Mater. Chem.*, 2009, **19**, 489–496.
29 H. Lian, Y. Dai, D. Yang, Z. Cheng, C. Li, Z. Hou, M. Shang and J. Lin, *Nanoscale*, 2014, **6**, 9703–9712.
30 A. Naduviledathu Raj, T. Rinkel and M. Haase, *Chem. Mater.*, 2014, **26**, 5689–5694.
31 H. Kobayashi, M. Ogawa, R. Alford, P. L. Choyke and Y. Urano, *Chem. Rev.*, 2010, **110**, 2620–2640.
32 C. Cao, W. Qin, J. Zhang, Y. Wang, P. Zhu, G. Wei, G. Wang, R. Kim and L. Wang, *Opt. Lett.*, 2008, **33**, 857–859.
33 M. Nyk, R. Kumar, T. Y. Ohulchanskyy, E. J. Bergey and P. N. Prasad, *Nano lett.*, 2008, **8**, 3834–3838.
34 G. Y. Chen, T. Y. Ohulchanskyy, R. Kumar, H. Agren and P. N. Prasad, *ACS Nano*, 2010, **4**, 3163–3168.

 